Nonequilibrium BCS State Dynamics Induced by Intense Terahertz Pulses in a Superconducting NbN Film

Ryusuke Matsunaga and Ryo Shimano
Department of Physics, The University of Tokyo, Tokyo, 113-0033, Japan
(Received 10 July 2012; published 31 October 2012)

Using terahertz (THz) pump-THz probe spectroscopy, we have investigated the dynamics of the nonequilibrium BCS state in a superconducting NbN film after the impulsive photoinjection of high-density Bogoliubov quasiparticles. The superconducting state rapidly changes within the duration of the monocycle THz pump pulse (1.6 ps). The complex optical conductivity spectrum in the nonequilibrium BCS state significantly deviates from that in the equilibrium state. The observed spectral features are qualitatively well described by the effective medium theory that assumes the formation of normal state patches embedded in a superconducting matrix.

DOI: 10.1103/PhysRevLett.109.187002 PACS numbers: 74.40.Gh, 74.25.Gz, 78.47.−p

The behavior of BCS superconducting states far from equilibrium has been a great focus of research for a long time [1,2] from the viewpoint of their fundamental interest and also their device application. Recently, intensive theoretical studies have been devoted to elucidate the fast time response of the BCS order to nonadiabatic perturbations. The damped or persistent oscillation of the BCS order parameter has been predicted in fermionic condensates after an abrupt change of their pairing interaction [3–5]. A similar temporal oscillation in the order parameter was also predicted to appear in conventional BCS superconductors (SCs) under the nonadiabatic excitation regime [6,7]. While the nonequilibrium BCS SCs have a long history of investigations, the fast dynamics caused by such an impulsive excitation in the time scale inverse of the BCS gap energy (typically 1 ps–1 THz in conventional SCs) has been unexplored due to the lack of experimental techniques. With recent progress in terahertz (THz) technology, however, a considerably strong THz pulse with the peak electric field (E field) as much as 1 MV/cm has been realized [8–11]. Accordingly, studies of nonlinear light-matter interactions in the THz range have been accelerated in various materials, e.g., in semiconductors [12–15], carbon nanotubes [16], and Mott insulators [17]. Nonlinear switching of Josephson plasma coupling in a high-T_c cuprate superconductor induced by the strong THz E field has also been reported [18]. In this Letter, we studied the ultrafast dynamics of the BCS state in a superconducting NbN film after the impulsive injection of Bogoliubov quasiparticles (QPs) at the edge of the BCS gap by using the intense THz pulse.

The mean-field theory of nonequilibrium superconductivity has shown that the injection of excess numbers of QPs induces a first-order phase transition from superconducting to normal metal phase [19]. The effect of external injection of QPs has been extensively studied by using superconducting tunnel-junction structures. The phase transition, the nonthermal energy distribution of QPs [20], and the formation of multigap states [21] have been revealed through the I-V characteristics of the tunnel junctions. The optical pump-probe method has also been performed to study the dynamics of nonequilibrium BCS states, in which QPs are injected into both the electronlike and holelike branches [22–28]. In the case of the near-visible pulse excitation, however, the hot electrons possessing huge excess energies emit large amounts of high-frequency phonons ($\hbar\omega \geq 2\Delta$). Therefore, the increase of the effective phonon temperature plays a crucial role in the optically excited nonequilibrium BCS state [29]. In contrast, intense THz pulses with their photon energy resonant to the BCS gap can cause the direct excitation of high-density QPs without heating the phonon subsystem.

Here we studied the ultrafast dynamics of the nonequilibrium BCS state in NbN induced by the intense THz pump pulse. We performed THz pump-THz probe spectroscopy to directly probe the ultrafast dynamics of the BCS gap in NbN, $2\Delta(0) = 5.2$ meV(= 1.3 THz), after the impulsive QP excitation. By using the intense THz pulse with the peak E field exceeding 50 kV/cm, the photoinjection of high-density QPs as much as $10^{20}/\mathrm{cm}^3$ is realized, even though the reflection loss of NbN is very high in the THz range [30]. We found that, after the intense THz pulse irradiation, superconductivity is rapidly switched off within the duration of the monocycle THz pulse. The spectral feature is reasonably reproduced by using the Bruggeman effective medium theory assuming that the system consists of the superconducting phase and the normal metal phase.

The sample was an epitaxial NbN film with 24-nm thickness grown on a 500-μm thick (100) MgO substrate by using the pulsed-laser deposition technique. Figures 1(a) and 1(b) show the temperature dependence of the complex optical conductivity $\sigma_1(\omega) + i\sigma_2(\omega)$ of the film, showing the BCS gap that opens below $T_c = 15.1$ K. The solid curves in Fig. 1 are calculated by the Mattis-Bardeen model [31,32]. As a light source, we used a regenerative

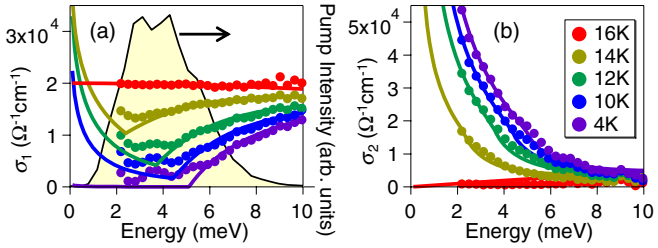

FIG. 1 (color online). (a),(b) The temperature dependence of the real- and imaginary-part optical conductivity spectra, respectively. The solid curves show the calculated spectra using the Mattis-Bardeen model. The shaded curve in (a) is the power spectrum of the pump THz pulse (right axis).

amplified Ti:sapphire laser system. The intense THz pump pulses were generated by the tilted-pulse-front method [8,9,16,33]. The power spectrum of the THz pump pulse is located at the BCS gap region of NbN as shown in Fig. 1(a) so that QPs are resonantly excited. The probe THz pulse was generated by the optical rectification in a ZnTe crystal. The pump and probe pulses collinearly enter the sample with polarizations orthogonal to each other [Fig. 2(a)]. The transmitted probe THz E field was detected by the free-space electro-optic sampling in a ZnTe crystal, while the pump pulse was blocked by a wire-grid polarizer placed after the sample. The details of the experimental method are described in the Supplemental Material [30].

By scanning both the delay time of the gate pulse for the electro-optic sampling of the probe THz pulse, t_{gate}, and the delay time of the probe to the pump THz pulse, t_{pp}, we performed the THz pump-THz probe spectroscopy. Figure 2(b) shows the probe THz E field E_{probe} transmitted through the sample at a temperature of 4 K as functions of t_{gate} and t_{pp} under the pump THz peak E field of 100 kV/cm. The diagonal dotted line indicates the remnant of the pump pulse. When the pump pulse temporally precedes the probe pulse, the waveform of the transmitted probe pulse is drastically changed. Figure 2(c) shows the waveform of the probe pulse in Fig. 2(b) before and after the pump pulse. Figure 2(d) shows the change of the probe E field $\Delta E_{\mathrm{probe}}$ induced by the pump pulse as functions of t_{gate} and t_{pp}. The pump-probe signal $\Delta E_{\mathrm{probe}}$ is observed only below T_c [30], indicating that the signal reflects the pump-induced nonequilibrium dynamics of the BCS state. Figure 2(e) shows the temporal evolution of $\sigma_1(\omega)$ at each t_{pp} obtained from Fig. 2(b). After the pump, we found a drastic increase of the optical conductivity below the BCS gap. The detailed spectral profile is discussed later (Fig. 4). Figure 2(f) shows the temporal evolution of σ_1 integrated from 2 to 5 meV in Fig. 2(e). For a reference, the change of the probe THz E field $\Delta E_{\mathrm{probe}}$ is also plotted in Fig. 2(f) at the fixed gate delay time $t_{\mathrm{gate}} = 0$. Since the evolution of $\sigma_1(\omega)$ below the gap is in good correspondence with that of $\Delta E_{\mathrm{probe}}$, we discuss the ultrafast dynamics of the nonequilibrium BCS state by using $\Delta E_{\mathrm{probe}}(t_{\mathrm{gate}} = 0)$.

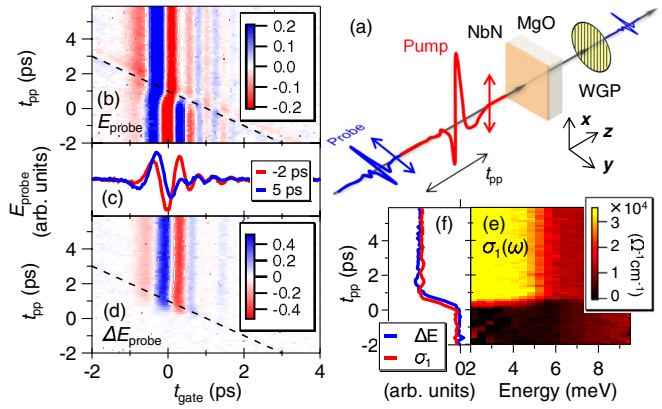

FIG. 2 (color online). (a) Schematics of the THz pump-THz probe spectroscopy. WGP: A wire-grid polarizer. (b) Mapping of the probe THz E field E_{probe} as functions of the gate delay time t_{gate} and the pump-probe delay time t_{pp} with the pump THz peak E field of 100 kV/cm at 4 K. The dotted line is a guide to the eye to indicate the trace of the pump THz pulse. (c) The waveforms of the probe THz pulse at $t_{\mathrm{pp}} = -2$ and 5 ps in (b). (d) Mapping of the change of E_{probe} induced by the THz pump, $\Delta E_{\mathrm{probe}}$. (e) The temporal evolution of the $\sigma_1(\omega)$ spectra obtained from (b). (f) The temporal evolution of $\Delta E_{\mathrm{probe}}(t_{\mathrm{gate}} = 0)$ and the integrated σ_1 from $\omega = 2$ to 5 meV as a function of t_{pp}.

Figure 3(a) shows the temporal evolution of $\Delta E_{\mathrm{probe}}(t_{\mathrm{gate}} = 0)$ at 4 K with various THz pump intensities as a function of t_{pp}. The pump THz E field is also shown in Fig. 3(a). $\Delta E_{\mathrm{probe}}$ rapidly increases right after the pump THz irradiation. After $t_{\mathrm{pp}} \sim 1.6$ ps, $\Delta E_{\mathrm{probe}}$ becomes constant, indicating that the nonequilibrium BCS state reaches a quasistable state. Note that the rising time of 1.6 ps corresponds to the single cycle of the pump THz

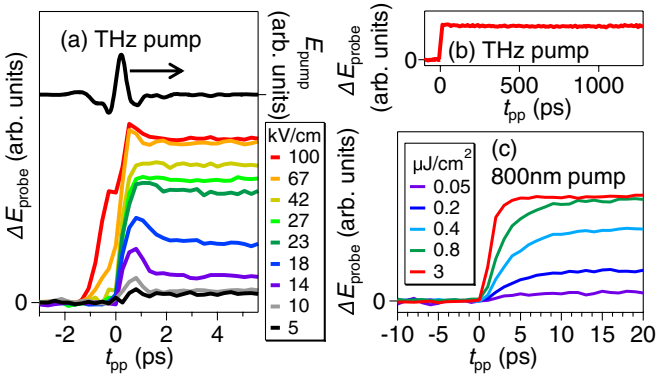

FIG. 3 (color online). (a) The temporal evolution of $\Delta E_{\mathrm{probe}}(t_{\mathrm{gate}} = 0)$ at 4 K for various THz pump intensities (left axis). The black curve shows the waveform of the E field of the pump THz pulse (right axis). (b) The temporal evolution of $\Delta E_{\mathrm{probe}}(t_{\mathrm{gate}} = 0)$ at 10 K with the pump THz E field of 100 kV/cm. (c) The temporal evolution of $\Delta E_{\mathrm{probe}}(t_{\mathrm{gate}} = 0)$ at 4 K in the case of the optical pump using the 800-nm femtosecond pulse.

pulse. Such a rapid change of the BCS state induced by the THz pump makes a contrast with the case of the near-visible optical pump case. Figure 3(c) shows the result of the optical pump-THz probe spectroscopy using the 800 nm pump pulse with 25-fs pulse duration. The rising time of $\Delta E_{\mathrm{probe}}$ strongly depends on the excitation intensity, varying from about 20 to 2 ps. This intensity-dependent rise time has been reported in the optical pump case and attributed to the thermalization dynamics between QPs, phonons, and Cooper pairs [27]. The optical pump generates hot electrons, and their excess energies are transferred to the creation of large amounts of high-frequency phonons, which in turn cause the pair breaking, resulting in the suppression of the superconductivity. In contrast, the THz pump pulse resonantly excites the low-energy QPs without the process of phonon emission from hot electrons. Therefore the observed ultrafast change of the BCS state, nearly independent of the pump THz intensity, is plausibly attributed to the direct photoinjection of QPs.

The decay time of $\Delta E_{\mathrm{probe}}$ ranges from several hundreds of picoseconds to more than 1 ns, depending on the temperature and the pump intensity, as shown in Fig. 3(b). Under the high-density condition, the lifetime of QPs due to their bimolecular recombination could be very short (< 1 ps) [25,27]. However, when two QPs recombine to a Cooper pair with emitting a high-frequency phonon, the emitted phonon in turn breaks a Cooper pair and two QPs are created again [34]. Thus, the recovery dynamics of the nonequilibrium BCS state is governed by not the QP recombination rate but rather the loss rate of the high-frequency phonons, i.e., the anharmonic decay or escape from the sample. This is referred to as the phonon-bottleneck effect, to which we attributed the observed long recovery time in Fig. 3(b). A similar behavior has also been reported in previous experiments [24–27]. As the pump THz intensity increases, $\Delta E_{\mathrm{probe}}(t_{\mathrm{pp}} > 1.6$ ps) is saturated. With further increasing the pump THz intensity, the rise of $\Delta E_{\mathrm{probe}}$ becomes earlier, indicating that the precursor part of the pump THz E field before the main peak induces the change of the BCS state in the strong excitation regime.

Figures 4(a) and 4(b) show the real- and imaginary-part optical conductivity spectra, respectively, 20 ps after the THz pump at 4 K. With increasing the pump intensity, $\sigma_1(\omega)$ below the gap energy significantly increases and far exceeds the value of the normal metallic state, while $\sigma_1(\omega)$ at the gap energy of $\sim$5 meV remains smaller than that of the normal state. Such a spectral profile of $\sigma_1(\omega)$ after the intense THz pulse irradiation is clearly different from that of the equilibrium states shown in Fig. 1(a). Thus the nonequilibrium BCS state caused by the high-density QP injection cannot be accounted for by the increase of the effective temperature which results in the continuous reduction of the BCS gap.

To understand the observed spectral behavior, we consider the spatial instability of the nonequilibrium

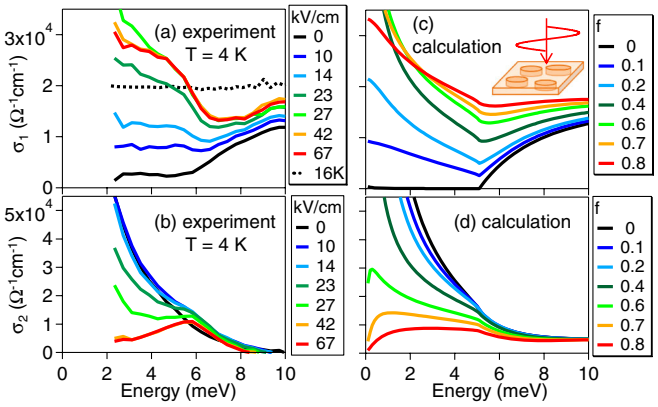

FIG. 4 (color online). (a),(b) The real- and imaginary-part optical conductivity spectra, respectively, at $t_{\mathrm{pp}} = 20$ ps for various THz excitation intensities at 4 K. For reference, $\sigma_1(\omega)$ in the normal metal state at 16 K is plotted as a dotted line. (c), (d) The calculated real- and imaginary-part optical conductivity spectra, respectively, using Eq. (1). The inset is a schematic image of the inhomogeneously suppressed superconductivity.

superconductivity. It is expected that, when the QP density exceeds a critical value, the higher-density region with the smaller gap energy becomes energetically more favorable for QPs, and the QPs flow into the higher-density region, resulting in a spatially inhomogeneous suppression of the superconductivity [35,36], with a length scale of the order of 1 μm expected for a NbN film [30]. In order to describe the electromagnetic response in such an inhomogeneous system, we use the Bruggeman effective medium theory (EMT) [37]. The EMT describes the effective dielectric function of composite materials where the size of the minor constituent is much smaller than the wavelength and has been applied to describe the SC-metal composites [38] and mixed states of type-II SCs [39,40]. Here we assume that the THz-induced nonequilibrium BCS state consists of the superconducting region and the nonsuperconducting region, which we call here hot spots. According to the EMT, the effective complex optical conductivity of the composite, $\sigma_{\mathrm{eff}}(\omega)$, satisfies the following equation:

$$f\frac{\sigma_h(\omega)-\sigma_{\mathrm{eff}}(\omega)}{g\sigma_h(\omega)+(1-g)\sigma_{\mathrm{eff}}(\omega)}+(1-f)\times\frac{\sigma_s(\omega)-\sigma_{\mathrm{eff}}(\omega)}{g\sigma_s(\omega)+(1-g)\sigma_{\mathrm{eff}}(\omega)}=0, \quad (1)$$

where $\sigma_h(\omega)$ and $\sigma_s(\omega)$ are the complex optical conductivities of the hot spot and superconducting state, respectively, f a volume fraction of the hot spots, and $g = 1/2$ a depolarization factor determined by the shape of the hot spots [30]. Figures 4(c) and 4(d) show the calculated real and imaginary parts of $\sigma_{\mathrm{eff}}(\omega)$, where $\sigma_h(\omega)$ and $\sigma_s(\omega)$ are calculated by the Mattis-Bardeen model with 16 and 4 K, respectively [31,32], assuming that the hot spots are regarded as normal metal. While the EMT can be applied in principle at all ranges of f in the small diameter limit

[41], as increasing the diameter the large filling factor f around 0.5 would make the EMT invalid, which might be the origin of the difference in Figs. 4(a) and 4(c). Nevertheless, the calculated spectra reproduce the experimental results well: (i) the anomalous increase of $\sigma_1(\omega)$ below the gap energy exceeding the value of the normal metal phase, (ii) suppression of $\sigma_2(\omega)$ below the gap energy which corresponds to the superfluid density, and (iii) the sustaining gap structure around the bare BCS gap energy. Therefore the BCS gap energy outside the hot spots is considered to maintain its initial values before the THz pump. The observed THz pump intensity dependence is accounted for by the increase of the volume fraction of the hot spots.

The QP condensation due to the intrinsic instability of the nonequilibrium superconductivity has been discussed based on the μ^* model [19], which describes the QP distribution by a Fermi-Dirac distribution function with an effective chemical potential μ^* and ambient temperature, assuming that the thermalization rate between QPs and phonons is much faster than the QP recombination rate. Whereas the intense THz pump generates the nonequilibrium distribution of QPs in the initial excitation process, the recombination time of QPs in the high-density regime is considered to overcome the thermalization time of QPs within the QPs branches, as discussed in Fig. 3(b) in terms of the phonon-bottleneck effect. Therefore, in the present situation, the local temperature of the QP condensation must be higher than the surrounding area. A similar local heating effect, although the initial process is different, has been discussed in the near-visible photon ($\hbar\omega \gg 2\Delta$) absorption experiment, where a large excess energy by each photon induces the multiple excitation of QPs and phonons and results in the formation of a nonsuperconducting region [42–44]. The scale of such a local heating area is related to ''thermal healing length,'' which is about several tens of nanometers [42–44]. Therefore, we consider that the spatial scale of the nonsuperconducting region is much smaller than the wavelength of the probe THz pulse of $\sim$300 μm and larger than the film thickness of 24 nm, even if the local heating of the nonsuperconducting area is taken into account.

Now we address the initial temporal behavior accompanied by an overshoot in $\Delta E_{\mathrm{probe}}$ in the weak excitation regime in Fig. 3(a). This transient peaklike signal of $\Delta E_{\mathrm{probe}}$ rapidly decays within 0.1–1 ps to the long-lasting quasistable value. As the pump intensity increases, the transient peaklike signal disappears. There are two possible scenarios as the origin of the peaklike signal: (i) The transient peak is associated with the process of the spatial condensation of QPs. However, as the pump intensity increases, the decay time of the transient peak becomes longer. This seems to be opposite to the interpretation of the spatial inhomogeneity, because the stronger excitation would induce more rapid condensation. (ii) The transient signal is related to the order parameter oscillation [6,7]. Since our results indicate that the spatial instability rapidly occurs in the strong THz excitation regime, the oscillation is expected to be limited only in the weak excitation regime. The damping of the predicted oscillation is proportional to $1/\sqrt{\Delta_\infty t}$ [4], where Δ_∞ is a constant value to which the order parameter asymptotes in the nonequilibrium BCS state. The stronger excitation would make Δ_∞ smaller, resulting in the long-surviving oscillation. The oscillatory structure of the order parameter is not observed in the present experiment, which suggests that the fast oscillation might be smeared out in the THz probe spectra as pointed out in Ref. [6]. Further experiments with a shorter THz pulse compared to the gap frequency, with its photon energy tuned near above the gap energy avoiding the injection of excess energy to the system, would resolve the origin of the initial overshoot signal.

In summary, we have investigated the ultrafast dynamics of the nonequilibrium BCS state induced by the intense THz pulse in superconducting NbN film. The complex optical conductivity spectra in the BCS gap region are qualitatively well reproduced by the effective medium theory that assumes the formation of normal state patches embedded in a superconducting matrix, which suggests an ultrafast suppression of superconductivity associated with the spatial condensation of QPs excited by the intense THz pulse. The THz pump-THz probe spectroscopy will be a promising tool to further explore the possibility of coherent control and/or phase transition in quantum phases with spontaneous symmetry breaking. The technique will also offer an understanding of the ultrafast response of superconductors to the THz photon and the dynamics of a hot spot which are crucial for device applications such as ultrasensitive THz photon detectors.

We thank M. Kawasaki for providing the NbN film sample and T. Oka and H. Aoki for helpful discussion. This work was partially supported by a Grant-in-Aid for Scientific Research (Grants No. 22244036 and No. 20110005) and by the Photon Frontier Network Program from MEXT, Japan.

[1] M. Tinkham, *Introduction to Superconductivity* (McGraw-Hill, New York, 1996).
[2] P. W. Anderson, Phys. Rev. **112**, 1900 (1958).
[3] R. A. Barankov, L. S. Levitov, and B. Z. Spivak, Phys. Rev. Lett. **93**, 160401 (2004).
[4] E. A. Yuzbashyan, O. Tsyplyatyev, and B. L. Altshuler, Phys. Rev. Lett. **96**, 097005 (2006).
[5] R. A. Barankov and L. S. Levitov, Phys. Rev. Lett. **96**, 230403 (2006).
[6] T. Papenkort, V. M. Axt, and T. Kuhn, Phys. Rev. B **76**, 224522 (2007).
[7] T. Papenkort, T. Kuhn, and V. M. Axt, Phys. Rev. B **78**, 132505 (2008).

[8] J. Hebling, G. Almasi, I. Kozma, and J. Kuhl, Opt. Express **10**, 1161 (2002).

[9] J. Hebling, K.-L. Yeh, M. C. Hoffmann, B. Bartal, and K. A. Nelson, J. Opt. Soc. Am. B **25**, B6 (2008).

[10] H. Hirori, A. Doi, F. Blanchard, and K. Tanaka, Appl. Phys. Lett. **98**, 091106 (2011).

[11] J. A. Fülöp, L. Pálfalvi, S. Klingebiel, G. Almási, F. Krausz, S. Karsch, and J. Hebling, Opt. Lett. **37**, 557 (2012).

[12] M. C. Hoffmann and J. A. Fülöp, J. Phys. D **44**, 083001 (2011).

[13] K. Tanaka, H. Hirori, and M. Nagai, IEEE Trans. Terahertz Sci. Technol. **1**, 301 (2011).

[14] W. Kuehn, P. Gaal, K. Reimann, M. Woerner, T. Elsaesser, and R. Hey, Phys. Rev. Lett. **104**, 146602 (2010).

[15] F. Blanchard *et al.*, Phys. Rev. Lett. **107**, 107401 (2011).

[16] S. Watanabe, N. Minami, and R. Shimano, Opt. Express **19**, 1528 (2011); **19**, 15 388 (2011).

[17] M. Liu *et al.*, Nature (London) **487**, 345 (2012).

[18] A. Dienst, M. C. Hoffmann, D. Fausti, J. C. Petersen, S. Pyon, T. Takayama, H. Takagi, and A. Cavalleri, Nature Photon. **5**, 485 (2011).

[19] C. S. Owen and D. J. Scalapino, Phys. Rev. Lett. **28**, 1559 (1972).

[20] S. B. Kaplan, J. R. Kirtley, and D. N. Langenberg, Phys. Rev. Lett. **39**, 291 (1977).

[21] I. Iguchi, S. Kotani, Y. Yamaki, Y. Suzuki, M. Manabe, and K. Harada, Phys. Rev. B **24**, 1193 (1981).

[22] J. F. Federici, B. Greene, P. Saeta, D. Dykaar, F. Sharifi, and R. Dynes, Phys. Rev. B **46**, 11 153 (1992).

[23] G. L. Carr, R. P. S. M. Lobo, J. LaVeigne, D. H. Reitze, and D. B. Tanner, Phys. Rev. Lett. **85**, 3001 (2000).

[24] Y. Xu, M. Khafizov, L. Satrapinsky, P. Kúš, A. Plecenik, and R. Sobolewski, Phys. Rev. Lett. **91**, 197004 (2003).

[25] J. Demsar, R. D. Averitt, A. J. Taylor, V. V. Kabanov, W. N. Kang, H. J. Kim, E. M. Choi, and S. I. Lee, Phys. Rev. Lett. **91**, 267002 (2003).

[26] R. P. S. M. Lobo, J. D. LaVeigne, D. H. Reitze, D. B. Tanner, Z. H. Barber, E. Jacques, P. Bosland, M. J. Burns, and G. L. Carr, Phys. Rev. B **72**, 024510 (2005).

[27] M. Beck, M. Klammer, S. Lang, P. Leiderer, V. V. Kabanov, G. N. Gol'tsman, and J. Demsar, Phys. Rev. Lett. **107**, 177007 (2011).

[28] R. D. Averitt and A. J. Taylor, J. Phys. Condens. Matter **14**, R1357 (2002).

[29] W. H. Parker, Phys. Rev. B **12**, 3667 (1975).

[30] See Supplemental Material at http://link.aps.org/supplemental/10.1103/PhysRevLett.109.187002 for the details of experimental methods and analysis.

[31] D. C. Mattis and J. Bardeen, Phys. Rev. **111**, 412 (1958).

[32] W. Zimmermann, E. H. Brandt, M. Bauer, E. Seider, and L. Genzel, Physica (Amsterdam) **183C**, 99 (1991).

[33] R. Shimano, S. Watanabe, and R. Matsunaga, J. Infrared Millim. Terahertz Waves **33**, 861 (2012).

[34] A. Rothwarf and B. N. Taylor, Phys. Rev. Lett. **19**, 27 (1967).

[35] J.-J. Chang and D. J. Scalapino, Phys. Rev. B **10**, 4047 (1974).

[36] D. J. Scalapino and B. A. Huberman, Phys. Rev. Lett. **39**, 1365 (1977).

[37] G. L. Carr, S. Perkowitz, and D. B. Tanner, J. Infrared Millim. Waves **13**, 171 (1985).

[38] J. Garner and D. Stroud, Phys. Rev. B **28**, 2447 (1983).

[39] Y. Ikebe, R. Shimano, M. Ikeda, T. Fukumura, and M. Kawasaki, Phys. Rev. B **79**, 174525 (2009).

[40] M. Šindler, R. Tesař, J. Koláček, L. Skrbek, and Z. Šimša, Phys. Rev. B **81**, 184529 (2010).

[41] G. A. Niklasson, C. G. Granqvist, and O. Hunderi, Appl. Opt. **20**, 26 (1981).

[42] A. M. Kadin and M. W. Johnson, Appl. Phys. Lett. **69**, 3938 (1996).

[43] G. N. Gol'tsman, O. Okunev, G. Chulkova, A. Lipatov, A. Semenov, K. Smirnov, B. Voronov, A. Dzardanov, C. Williams, and R. Sobolewski, Appl. Phys. Lett. **79**, 705 (2001).

[44] A. D. Semenov, G. N. Gol'tsman, and A. A. Korneev, Physica (Amsterdam) **351C**, 349 (2001).